

## Journal Pre-proofs

Utilizing Structure Based Drug Design and Metabolic Soft Spot Identification to optimize the *in vitro* potency and *in vivo* Pharmacokinetic Properties Leading to the Discovery of Novel Reversible Bruton's Tyrosine Kinase Inhibitors

Brian T. Hopkins, Eris Bame, Noah Bell, Tonika Bohnert, Jon K. Bowden-Verhoek, Minna Bui, Mark T. Cancilla, Patrick Conlon, Patrick Cullen, Daniel A. Erlanson, Junfa Fan, Tarra Fuchs-Knotts, Stig Hansen, Stacey Heumann, Tracy J. Jenkins, Chuck Gua, Ying Yiu, YuTing Liu, Mukush Lulla, Douglas Marcotte, Isaac Marx, Bob McDowell, Elisabeth Mertsching, Ella Negrou, Michael J. Romanowski, Daniel Scott, Laura Silvian, Wenjin Yang, Min Zhong

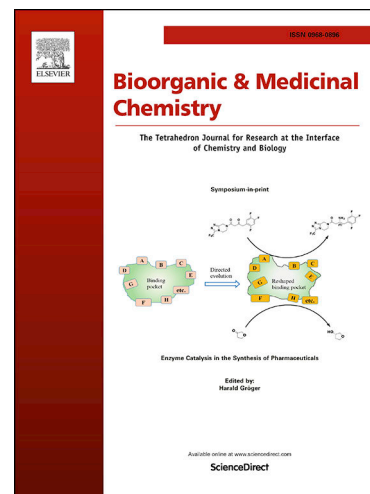
PII: S0968-0896(21)00283-2  
DOI: <https://doi.org/10.1016/j.bmc.2021.116275>  
Reference: BMC 116275

To appear in: *Bioorganic & Medicinal Chemistry*

Received Date: 4 March 2021  
Revised Date: 4 June 2021  
Accepted Date: 9 June 2021

Please cite this article as: B.T. Hopkins, E. Bame, N. Bell, T. Bohnert, J.K. Bowden-Verhoek, M. Bui, M.T. Cancilla, P. Conlon, P. Cullen, D.A. Erlanson, J. Fan, T. Fuchs-Knotts, S. Hansen, S. Heumann, T.J. Jenkins, C. Gua, Y. Yiu, Y. Liu, M. Lulla, D. Marcotte, I. Marx, B. McDowell, E. Mertsching, E. Negrou, M.J. Romanowski, D. Scott, L. Silvian, W. Yang, M. Zhong, Utilizing Structure Based Drug Design and Metabolic Soft Spot Identification to optimize the *in vitro* potency and *in vivo* Pharmacokinetic Properties Leading to the Discovery of Novel Reversible Bruton's Tyrosine Kinase Inhibitors, *Bioorganic & Medicinal Chemistry* (2021), doi: <https://doi.org/10.1016/j.bmc.2021.116275>

This is a PDF file of an article that has undergone enhancements after acceptance, such as the addition of a cover page and metadata, and formatting for readability, but it is not yet the definitive version of record. This version will undergo additional copyediting, typesetting and review before it is published in its final form, but we are providing this version to give early visibility of the article. Please note that, during the production process, errors may be discovered which could affect the content, and all legal disclaimers that apply to the journal pertain.



Journal Pre-proofs

## Graphical Abstract

To create your abstract, type over the instructions in the template box below.  
Fonts or abstract dimensions should not be changed or altered.

### **Utilizing Structure Based Design and Metabolic Soft Spot Identification to Optimize the *in vitro* Potency and *in vivo* Pharmacokinetic Properties Leading to the Discovery of novel Reversible Bruton's Tyrosine Kinase Inhibitors.**

Leave this area blank for abstract info.

Brian T. Hopkins<sup>a</sup>, \* Eris Bame<sup>a</sup>, Noah Bell<sup>b</sup>, Tonika Bohnert<sup>a</sup>, Jon K. Bowden-Verhoek<sup>a</sup>, Minna Bui<sup>b</sup>, Mark T. Cancilla<sup>b</sup>, Patrick Conlon<sup>a</sup>, Patrick Cullen<sup>a</sup>, Daniel A. Erlanson<sup>b</sup>, Junfa Fan<sup>b</sup>, Tarra Fuchs-Knotts<sup>b</sup>, Stig Hansen<sup>b</sup>, Stacey Heumann<sup>b</sup>, Tracy J. Jenkins<sup>a</sup>, Chungang Gu<sup>a</sup>, Ying Yiu<sup>a</sup>, YuTing Liu<sup>a</sup>, Mukush Lulla<sup>a</sup>, Douglas Marcotte<sup>a</sup>, Isaac Marx<sup>a</sup>, Bob McDowell<sup>b</sup>, Elisabeth Mertsching<sup>a</sup>, Ella Negrou<sup>a</sup>, Michael J. Romanowski<sup>b</sup>, Daniel Scott<sup>a</sup>, Laura Silvian<sup>a</sup>, Wenjin Yang<sup>b</sup>, Min Zhong<sup>b</sup>.

<sup>a</sup> Biogen Inc., 225 Binney Street, Cambridge, MA 02142, United States.

<sup>b</sup> Sunesis Pharmaceuticals, Inc. 395 Oyster Point Boulevard, South San Francisco, CA 94080, United States



## Utilizing Structure Based Drug Design and Metabolic Soft Spot Identification to optimize the *in vitro* potency and *in vivo* Pharmacokinetic Properties Leading to the Discovery of Novel Reversible Bruton's Tyrosine Kinase Inhibitors.

Brian T. Hopkins<sup>a</sup>, \* Eris Bame<sup>a</sup>, Noah Bell<sup>b</sup>, Tonika Bohnert<sup>a</sup>, Jon K. Bowden-Verhoek<sup>a</sup>, Minna Bui<sup>b</sup>, Mark T. Cancilla<sup>b</sup>, Patrick Conlon<sup>a</sup>, Patrick Cullen<sup>a</sup>, Daniel A. Erlanson<sup>b</sup>, Junfa Fan<sup>b</sup>, Tarra Fuchs-Knotts<sup>b</sup>, Stig Hansen<sup>b</sup>, Stacey Heumann<sup>b</sup>, Tracy J. Jenkins<sup>a</sup>, Chuck Gua<sup>a</sup>, Ying Yiu<sup>a</sup>, YuTing Liu<sup>a</sup>, Mukush Lulla<sup>a</sup>, Douglas Marcotte<sup>a</sup>, Isaac Marx<sup>a</sup>, Bob McDowell<sup>b</sup>, Elisabeth Mertsching<sup>a</sup>, Ella Negrou<sup>a</sup>, Michael J. Romanowski<sup>b</sup>, Daniel Scott<sup>a</sup>, Laura Silvian<sup>a</sup>, Wenjin Yang<sup>b</sup>, Min Zhong<sup>b</sup>.

<sup>a</sup> Biogen Inc., 225 Binney Street, Cambridge, MA 02142, United States.

<sup>b</sup> Sunesis Pharmaceuticals, Inc. 395 Oyster Point Boulevard, South San Francisco, CA 94080, United States

### ARTICLE INFO

#### Article history:

Received  
Received in revised form  
Accepted  
Available online

#### Keywords:

Bruton's Tyrosine Kinase (BTK)  
Fragment based screen, Computer aid drug design (CADD), Met ID, Metabolic Soft Spot Switching

### ABSTRACT

Bruton's tyrosine kinase (BTK) is an essential node on the BCR signaling in B cells, which are clinically validated to play a critical role in B-cell lymphomas and various auto-immune diseases such as Multiple Sclerosis (MS), Pemphigus, and rheumatoid arthritis (RA). Although non-selective irreversible BTK inhibitors have been approved for oncology, due to the emergence of drug resistance in B-cell lymphoma associated with covalent inhibitor, there an unmet medical need to identify reversible, selective, potent BTK inhibitor as viable therapeutics for patients. Herein, we describe the identification of Hits and subsequence optimization to improve the physicochemical properties, potency and kinase selectivity leading to the discovery of a novel class of BTK inhibitors. Utilizing Met ID and structure base design inhibitors were synthesized with increased *in vivo* metabolic stability and oral exposure in rodents suitable for advancing to lead optimization.

© 2019 Elsevier Ltd. All rights reserved.

\* Corresponding author. E-mail address: [Brian.Hopkins@biogen.com](mailto:Brian.Hopkins@biogen.com)

Bruton's tyrosine kinase, a member of the Tec protein tyrosine kinase (PTK)<sup>1</sup> family, is critical for B cell development. More than two decades ago, mutants in the BTK gene<sup>2-3</sup> on the X chromosome were found to be responsible for XLA patients' inability to develop an adaptive immune response to opportunistic infections. This genetic validation of BTK as a target for modulating B cell development set the stage for identification of small molecules BTK inhibitors as therapeutics for treatment of auto-immune diseases such as rheumatoid arthritis (RA),<sup>4</sup> multiple sclerosis (MS),<sup>5-6</sup> and B cell malignancies.<sup>7</sup>

In 2013 the FDA approved ibrutinib,<sup>8</sup> a covalent BTK inhibitor for the treatment of chronic lymphocytic leukemia (CLL) and mantle cell lymphoma (MCL). Subsequently in 2017 and 2019 acalabrutinib<sup>9</sup> and zanubrutinib<sup>10</sup> were approved to treat CLL and MCL as next generation irreversible BTK inhibitors exhibiting superior clinical safety and tolerability due to their improved kinase selectivity profiles. Although targeting BTK with covalent inhibitors has proven successful, an unmet medical need has emerged for new drugs which can target both the native and mutant BTK protein (Cys-481 versus Ser-481), which has been demonstrated to confer resistance<sup>11</sup> associated with chronic dosing of ibrutinib in patients. Thus, within the pharmaceutical industry substantial resources have been deployed to identify reversible drug candidates which do not require Cys-481 for activity, thereby avoiding the potential for drug resistance due to site mutations in the BTK kinase domain. To date six novel reversible BTK candidates, fenebrutinib (GDC-0853),<sup>12</sup> vecabrutinib (SNS-062),<sup>13</sup> BIIB068,<sup>14</sup> BMS-986142,<sup>15</sup> ARQ531,<sup>16</sup> AS-871<sup>17-18</sup> and LOXO-305,<sup>19</sup> have advanced to the clinic for treatment of oncology and auto-immune diseases such as systemic lupus erythematosus (SLE), rheumatoid arthritis (RA), and multiple sclerosis (MS).<sup>20</sup>

## Results and discussion

Previously we reported<sup>21</sup> the utilization of a tethering fragment-based screen which resulted in the identification of novel low molecular weight hits which bound to BTK in a reversible fashion as shown in Scheme 1. These hits were subsequently optimized to improve both the *in vitro* potency and ADME properties leading to the discovery of **2**. This molecule was deprioritized based on an unacceptably high predicted human dose.<sup>22</sup> It was hypothesized that optimizing the physicochemical properties, in particular focusing on increasing the Fsp<sup>3</sup> character,<sup>23</sup> could increase the solubility and *in vitro* cellular potency leading to improved drug-like-properties and lowering the human predicted dose required for efficacy to afford a potential candidate suitable for advancing into development.

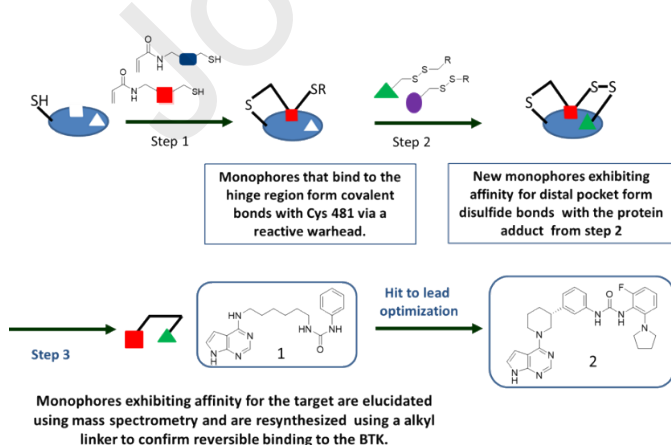
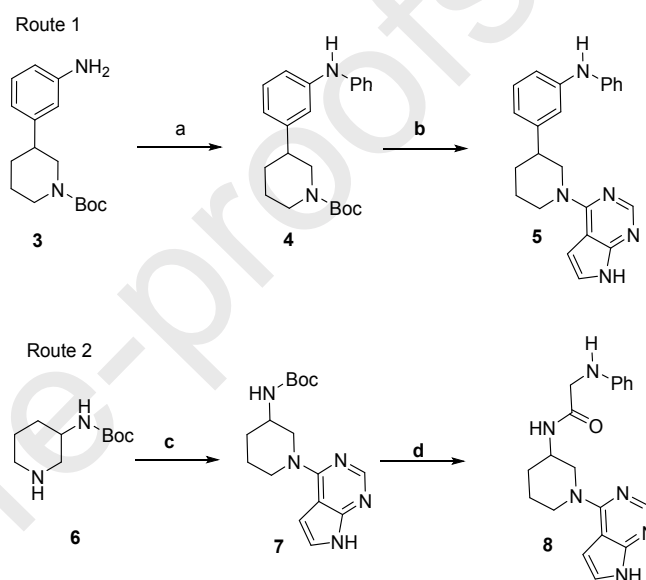


Figure 1. Summary of fragment-based screen to identify novel BTK hits.

To improve the drug-like properties, the central phenyl and urea motifs were targeted for removal. The crystal structure of **2** indicated the urea moiety made a H-bond with Asp-539 while orienting the substituted distal phenyl motif to extend into the "H3" pocket.<sup>21</sup> Utilizing *in silico* docking studies, a number of structurally diverse molecules were designed which exhibited binding poses enabling interactions with both the hinge region and the Asp-539 residue. For example, replacing the di-aryl urea moiety with the diarylamine motif was anticipated to preserve the key H-bond interaction with Asp-539, although the docking studies indicated the distal phenyl would be oriented away from Tyr-551. Similarly, replacing the central phenyl moiety with a flexible glycine linker was predicted to maintain the H-bond interaction with Asp-539 while again positioning the distal phenyl moiety away from the "H3" pocket.

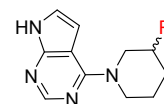


**Scheme 1. Reagents and conditions:** (a) Pd(OAc)<sub>2</sub>, BINAP, *t*-BuONa, 24 hr, 80 °C, 68% yield; (b) i. HCl, 1,4-Dioxane, 24 hr, rt; ii. 4-Chloro-7H-pyrrolo[2,3-*d*]pyrimidine, DIEA, DMF, 100 °C, 6 hr, 83% yield; (c) 4-Chloro-7H-pyrrolo[2,3-*d*]pyrimidine, DIEA, DMF, 100 °C, 6 hr, 87% yield; (d) i. HCl, 1,4-Dioxane, 24 hr, rt; ii. PhNHCH<sub>2</sub>CO<sub>2</sub>H, EDCI, HOBt, DIEA, DMF, 1 hr, rt, 81% yield.

Two synthetic routes were devised to enable the synthesis of both targets in 3 steps starting from readily available starting materials **3** and **6**. The bi-aryl amine **5** was synthesized utilizing a Buchwald-Hartwig coupling<sup>24</sup> of the aniline **3** with palladium acetate and BINAP to afford the bi-aryl amine intermediate **4** in 68% yield. The Boc group was removed under acidic conditions and the product was reacted with 4-chloro-pyrrolopyrimidine in the presence of excess DIEA to give **5** in 56% yield from **3**. For the synthesis of the glycine analog **8**, coupling of the commercially available *tert*-butyl piperidin-3-ylcarbamate **6** and 4-chloro-pyrrolo-pyrimidine afforded intermediate **7**, and removal of the Boc group followed by amide coupling using EDCI/HOBt gave **8** in 71% yield for the 3 steps.

## 2. Hit to lead optimization

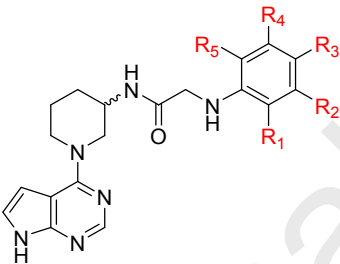
Table 1. BTK IC<sub>50</sub> values for derivatives containing alkyl and aryl linkers.



With a viable synthetic route in hand, it was feasible to determine whether replacing the original bi-aryl urea core with either the bi-aryl anine or glycine moieties would afford active molecules as predicted by the *in silico* docking studies. Although the observed affinity for **5** (BTK IC<sub>50</sub> = 2.8 μM) was 3-fold weaker than **9** (BTK IC<sub>50</sub> = 0.8 μM), this finding was encouraging as it confirmed that the key H-bond interaction with Asp-539 could be achieved using other functional group beside the urea moiety **9**. To further improve the potency for the new lead **5**, a series of *ortho*, *meta* and *para* substituted trifluoromethyl anilines were synthesized as it was hypothesized that the distal phenyl motif was binding in a putative lipophilic region. Unfortunately, analogs **10**, **11** and **12** did not show an improvement in biochemical potency compared to **5**.

In a similar fashion a series of glycine analogs containing a trifluoromethyl group at the *ortho*, *meta* and *para* position on the distal phenyl were synthesized. To our delight the original glycine analog **8** showed a 2-fold improvement in potency compared to the urea lead **9**. Furthermore, in contrast to the bi-aryl amine series, introducing a lipophilic trifluoromethyl group<sup>25</sup> at either the *ortho* (**13**) or *meta* (**14**) position exhibited improved potency, although a significant loss in activity was observed with the *para* substituted trifluoromethyl analog (**15**) which was attributed to unfavorable steric interactions within the active site. The stage was now set to further optimize the potency and drug-like properties for this novel glycine containing series.

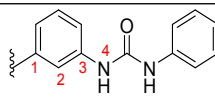
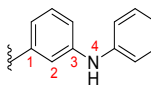
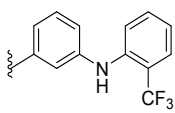
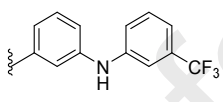
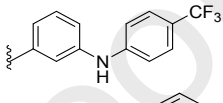
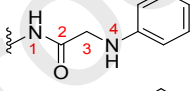
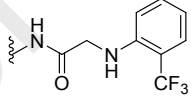
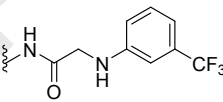
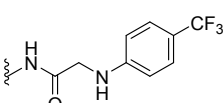
**Table 2.** Enzyme activity for analogs with various aryl substituents.



| Compd #   | Regio-substitutions |                |                                  |                |                 | BTK IC <sub>50</sub> (μM) <sup>a</sup> |
|-----------|---------------------|----------------|----------------------------------|----------------|-----------------|--|
|           | R <sub>1</sub>      | R <sub>2</sub> | R <sub>3</sub>                   | R <sub>4</sub> | R <sub>5</sub>  |  |
| <b>8</b>  | R/S                 | H              | H                                | H              | H               | 0.4                                    |
| <b>14</b> | R/S                 | H              | CF <sub>3</sub>                  | H              | H               | 0.12                                   |
| <b>16</b> | R/S                 | H              | C(CH <sub>3</sub> ) <sub>3</sub> | H              | H               | 0.71                                   |
| <b>17</b> | R/S                 | H              | CN                               | H              | H               | 1.7                                    |
| <b>18</b> | R/S                 | H              | SO <sub>2</sub> CF <sub>3</sub>  | H              | H               | 0.86                                   |
| <b>19</b> | R/S                 | H              | OCF <sub>3</sub>                 | H              | H               | 5.4                                    |
| <b>20</b> | R/S                 | H              | F                                | H              | H               | 0.11                                   |
| <b>21</b> | R/S                 | H              | Cl                               | H              | H               | 0.08                                   |
| <b>22</b> | R/S                 | F              | Cl                               | H              | H               | 0.22                                   |
| <b>23</b> | R/S                 | H              | Cl                               | F              | H               | 1.4                                    |
| <b>24</b> | R/S                 | H              | Cl                               | H              | F               | 0.036                                  |
| <b>25</b> | R/S                 | H              | Cl                               | H              | F               | 0.91                                   |
| <b>26</b> | R/S                 | H              | Cl                               | H              | Cl              | 0.019                                  |
| <b>27</b> | R/S                 | H              | Cl                               | H              | CF <sub>3</sub> | 0.041                                  |
| <b>28</b> | R                   | H              | Cl                               | H              | Cl              | 0.011                                  |

<sup>a</sup>IC<sub>50</sub> values were determined using non-phosphorylated protein in a FRET assay.

Compound **14** represented a new chemical class with improved physicochemical properties and lipophilic ligand efficacy<sup>26-28</sup> (**14** LLE = 3.9 *versus* **9** LLE = 1.9). However, anilines have been reported to exhibit a positive signal for genotoxicity in the AMES assay,<sup>29-31</sup> so it was deemed necessary to devise a strategy for derisking the aniline moiety. Our initial attempts to replace the

| #         | R   | IC <sub>50</sub> (μM) <sup>a</sup> |
|-----------|---|------------------------------------|
| <b>9</b>  |    | 0.8                                |
| <b>5</b>  |    | 2.8                                |
| <b>10</b> |    | >20                                |
| <b>11</b> |    | 4.7                                |
| <b>12</b> |    | >20                                |
| <b>8</b>  |    | 0.39                               |
| <b>13</b> |    | 0.34                               |
| <b>14</b> |   | 0.12                               |
| <b>15</b> |  | 5.6                                |

phenyl group with 5- or 6-membered heteroaryl moieties such as pyridyl, pyridinyl, triazoles or cycloalkyl motifs all resulted in a loss in affinity (BTK IC<sub>50</sub> > 10 μM) compared to compound **8** (see supplemental data). Thus, being unsuccessful in identifying a suitable replacement for the aniline moiety, the focus switched to mitigating the risk associated with this potential toxicophore.<sup>29-30</sup> Since the preliminary SAR indicated that substituents at the *meta* positions would be preferable, a series of commercially available *meta* substituted anilines were selected to probe the SAR within this region of the protein. Introducing polar substituents such as a nitrile **17**, or trifluoromethylsulfone **18**, resulted in a > 5 fold loss in potency, while lipophilic moieties such as fluoro<sup>32</sup> or chloro substituents exhibited comparable potency to **8**. With the discovery of the *meta* chloro analog **21** exhibiting a BTK IC<sub>50</sub> = 0.08 μM as a racemic mixture, the team focused on further improving the potency by incorporating a second substituent at either the 1, 3, 4 or 5 position on the phenyl moiety. Introducing a lipophilic substituent such as a fluoro atom at the 2, 4 or 6 positions led to a loss in potency, while a modest 2-fold increase in potency was observed with the 3-chloro-5-fluorophenyl analog **24**. To capitalize on this result two analogs containing the 3,5-dichloro and the 3-chloro-5-trifluoromethyl substituted aniline were synthesized to afford **26** and **27** which exhibited similar biochemical potency (BTK IC<sub>50</sub> = 0.019 μM and BTK IC<sub>50</sub> = 0.041 μM respectively) as observed with **24**. To confirm the absolute stereochemistry required for activity, both the R and S enantiomers were synthesized to afford the eutomer **28** with good biochemical potency (BTK IC<sub>50</sub> = 0.011 μM) and >20 fold selectivity versus other members of the Tec family (TEC IC<sub>50</sub> = 0.13 μM, ITK IC<sub>50</sub> = 0.23 μM, TXK IC<sub>50</sub> = 2.9 μM and BMX IC<sub>50</sub> = 0.94 μM). Incorporating the 3,5-dichloroaniline moiety improved the

inhibition of B cell proliferation  $IC_{50} = 1.2 \mu\text{M}$ ). In addition, the genotoxic risk was mitigated as the 3,5-dichloroaniline<sup>33-34</sup> had been reported to be negative for mutagenicity when tested in an AMES assay.

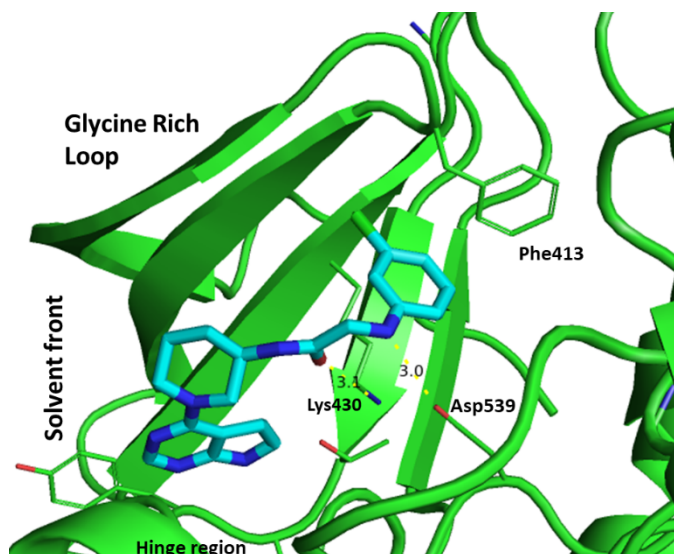
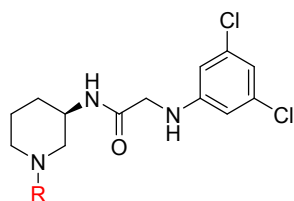


**Fig. 2.** Co-crystal structure of compound **21** bound in the BTK kinase domain.

A 1.8 Å co-crystal structure (Fig. 2.) of **21** bound to Btk showed the pyrrolopyrimidine binding to the hinge region with the pyrrole ring oriented towards the Thr gatekeeper and facilitating key hydrogen bond interactions with both Tyr-475 and Glu-475. The piperidine ring occupied the ribose pocket and appeared to be making hydrophobic interactions with the glycine-rich loop. As the molecule extended further into the ATP pocket, the glycine linker was ideally positioned to act as a dual hydrogen bond donor/acceptor with both the catalytic Lys-430 and Asp-539 and oriented the distal phenyl ring to bind in a putative hydrophobic region away from Tyr-551. Further analysis revealed that the distal aryl was making a face to edge  $\pi$  interaction with Phe 413 and the 3-chloro substituent was rotated toward the p-loop region.

With an understanding of the pharmacophore required for affinity, the focus shifted towards utilizing the crystal structure to improve the *in vitro* potency while optimizing the ADME properties. From an ADME perspective, it was anticipated that the pyrrolopyrimidine hinge binder would be a potential metabolic soft spot for this series as it was reported in the literature to undergo metabolic oxidation on the pyrrole ring.<sup>35</sup> Thus, to assess the liver microsomal stability, a series of analogs were synthesized to explore alternative hinge binders which would maintain the key H-bond donor/acceptor while attempting to reduce the electron rich character of this motif.

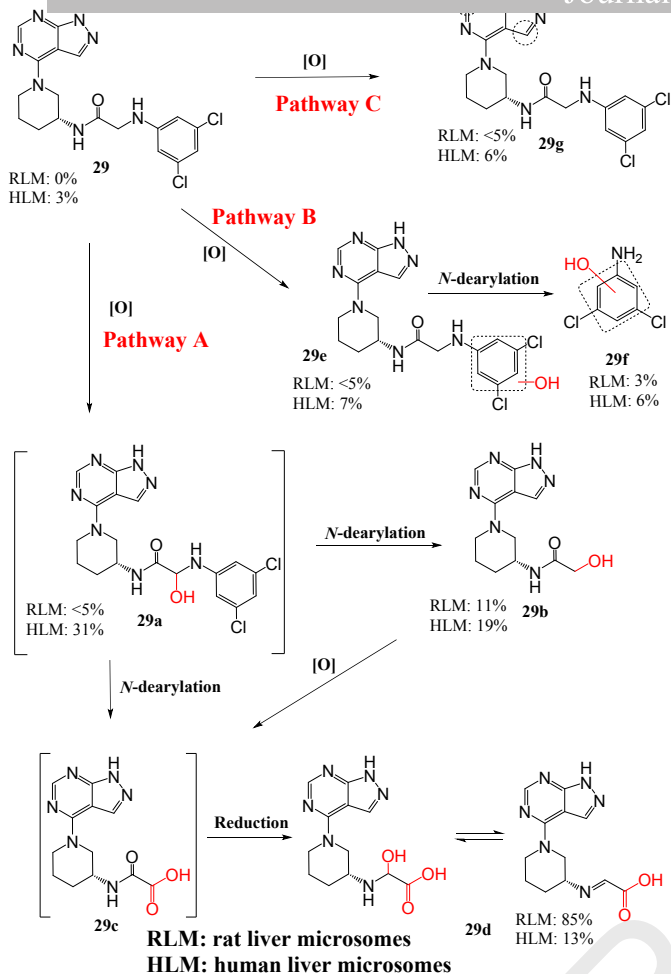
**Table 3.** Enzyme activity for analogs with different hinge binding motifs.



| Compound # | R | $IC_{50}$ ( $\mu\text{M}$ ) <sup>a</sup> | proliferation $IC_{50}$ ( $\mu\text{M}$ ) <sup>b</sup> | HLM CL % $Q_H$ <sup>c</sup> |
|------------|---|--|--|-----------------------------|
| 28         |   | 0.01                                     | 1.2  | >95, >95                    |
| 29         |   | 0.01                                     | 0.5  | >95, >95                    |
| 30         |   | 0.13                                     | 7.0  | >95, >95                    |
| 31         |   | 0.067                                    | 3.8  | >95, >95                    |
| 32         |   | 1.0                                      | NA   | >95, >95                    |
| 33         |   | 0.48                                     | >10  | NA                          |

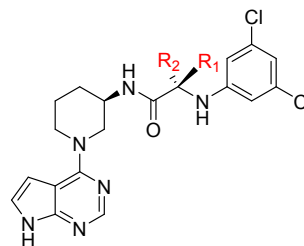
<sup>a</sup> $IC_{50}$  values were determined using non-phosphorylated BTK protein in a FRET assay. <sup>b</sup> $IC_{50}$  for B-cell proliferation were measured. Peripheral blood mononuclear cell (PBMC's). <sup>c</sup>Predicted hepatic oxidative clearance was measured in liver microsomal fraction,  $Q_H$  hepatic blood flow (portal vein plus hepatic artery).

Replacing the pyrrolopyrimidine hinge binder with the pyrazolopyrimidine afforded **29** which exhibited similar biochemical potency and a modest increase in cellular potency (B cell proliferation  $IC_{50} = 1.2$  vs  $0.5 \mu\text{M}$ ), but no improvement in the microsomal stability was observed. Since the pyrrolopyrimidine hinge binder was presumed to be metabolized *via* oxidation at the C6 position, we synthesized **30** containing the 5,7-dihydro-6H-pyrrolopyrimidin-6-one hinge binder. Unfortunately, this modification led to a loss in biochemical potency and demonstrated no improvement in the *in vitro* human liver microsomal stability (HLM). Finally, a series of monocyclic hetero-aryl analogs containing the H-bond donor were synthesized and shown to be less potent in the biochemical assay (BTK  $IC_{50} = 0.067 \mu\text{M}$  (**31**), BTK  $IC_{50} = 1.0 \mu\text{M}$  (**32**), BTK  $IC_{50} = 0.48 \mu\text{M}$  (**33**)) and did not exhibit any improvements in microsomal stability when tested in the *in vitro* RLM or HLM assays.



Since the Met ID studies highlighted pathway A as a major route of clearance in both rat and human liver microsomes, we explored the SAR on the central region of the molecule. Based on the analysis of the BTK co-crystal structures it was envisioned that introducing a substituent on the alpha carbon of the glycine linker may block metabolism at this central linker region while affording improvement in potency *via* introducing conformational constraints into the flexible linker region. To evaluate this, a series of chiral *N*-aryl- $\alpha$ -amino acids building blocks were synthesized *via* Ullmann couplings, followed by treatment with the 3-aminopiperidine moiety as described in Scheme 2 to afford a series of analogs shown in Table 3.

**Table 3.** Summary of *in vitro* biological potency and metabolic stability for analogs with substituents on the glycine linker.



| Cmpd # | R <sub>1</sub> | R <sub>2</sub> | BTK IC <sub>50</sub> ( $\mu$ M) <sup>a</sup> | B cell IC <sub>50</sub> ( $\mu$ M) <sup>b</sup> | H, R, LM %Q <sub>H</sub> <sup>c</sup> | LLE |
|--------|----------------|----------------|--|---|---------------------------------------|-----|
| 28     | H              | H              | 0.01   | 1.2   | >95                                   | 3.9 |
| 37     | Me             | H              | 0.014  | 1.3   | >95                                   | 3.5 |
| 38     | H              | Me             | >10  | -   | -                                     | -   |
| 39     | Me             | Me             | >10  | -   | -                                     | -   |
| 40     | Et             | H              | 0.005  | 0.46  | >95                                   | 3.4 |
| 41     |                | H              | 0.011  | 0.4   | >95                                   | 3.4 |
| 42     |                | H              | 0.005  | 0.8   | >95                                   | 3.0 |
| 43     |                | H              | 0.06   | 5.0   | >95                                   | 3.5 |
| 44     |                | H              | 1.5  | Na  | >95                                   | 2.8 |

<sup>a</sup>IC<sub>50</sub> values were determined using non-phosphorylated BTK protein in a FRET assay. <sup>b</sup>IC<sub>50</sub> for B-cell proliferation were measured. Peripheral blood mononuclear cell (PBMC's). <sup>c</sup>Predicted hepatic oxidative clearance was measured in human and rat liver microsomal (LM) fraction, Q<sub>H</sub> hepatic blood flow (portal vein plus hepatic artery).

**Fig. 3.** *In vitro* Met ID profile for compound 29 incubated with human and rat liver microsomes. All % values are relative LCMS peak areas after 30 minutes incubation of 29.

To establish an *in vitro-in vivo* correlation (IVIVC) for this series, compounds 28 and 29 were dosed IV at 1 mg/kg in 40% NMP in Sprague Dawley rats and exhibited high plasma clearance (CL %Q<sub>H</sub> = >100) consistent with the *in vitro* RLM data. In addition, metabolite identification (Met ID) studies were completed to elucidate potential metabolic soft spots attributed to the high *in vivo* clearance. The *in vitro* studies highlighted two major pathways for the oxidative metabolism for this series (Figure 3). In both HLM and RLM the major route of metabolism was *via* pathway A, involving oxidation of the glycine linker to afford the hemiaminal 29a and subsequent de-alkylation and reduction to afford 29b. In addition, oxidation of both the distal phenyl and the hinge binder motifs was observed presumably *via* pathways B and C respectively.

*in vitro* liver microsomal stability, hydrophobic and polar moieties such as ethyl **40**, cyclopropyl **41** or the iso-propyl **43** led to analogs with improved cellular potency while maintaining acceptable ligand efficiency (LLE). In addition to improving potency, introducing the alpha cyclopropyl substituent **41** exhibited modest off-target selectivity when profiled in the DiscoverX kinome panel (42/410 with > 90% inhibition at 10  $\mu$ M) and > 10 fold selectivity over the Tec family members (TEC  $K_d$  = 0.051  $\mu$ M, TXK  $K_d$  = 0.86  $\mu$ M, ITK  $K_d$  = 0.021  $\mu$ M, BMX  $K_d$  = 3.8  $\mu$ M). To understand how the binding to BTK was influencing the overall kinome selectivity for this series, we decided to first identify the key differences within the sequences across the Tec family members which explained the selectivity profiled observed with this series of compounds.

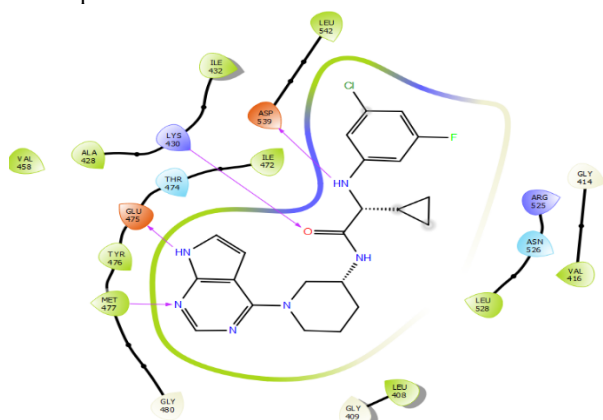


Fig. 4 Illustration of compound **45** bound in the BTK active site.

Table 4 Comparing residues within the BTK protein with other TEC family members.

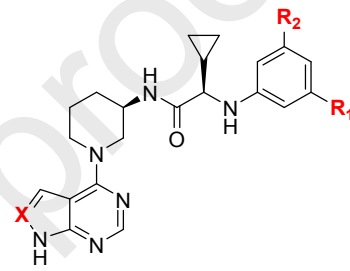
| Domain | Residue          | Kinase |                |                |                |                |
|--------|------------------|--------|----------------|----------------|----------------|----------------|
|        |                  | BTK    | TEC            | TXK            | BMX            | ITK            |
| B4     | 428              | A      | A              | A              | A              | A              |
|        | 430 <sup>b</sup> | K      | K              | K              | K              | K              |
| BAC    | 432 <sup>c</sup> | I      | I              | I              | I              | I              |
| GRL    | 408              | L      | L              | I <sup>d</sup> | L              | I <sup>d</sup> |
|        | 409              | G      | G              | G              | G              | G              |
|        | 414              | G      | G              | G              | G              | G              |
|        | 415              | V      | V              | V              | V              | L <sup>d</sup> |
| UPH    | 416              | V      | V              | V              | V              | V              |
|        | 472              | I      | I              | I              | I              | L              |
|        | 474 <sup>a</sup> | T      | T              | T              | T              | F <sup>d</sup> |
|        | 475              | E      | E              | E              | E              | E              |
|        | 476              | Y      | F <sup>d</sup> | F <sup>d</sup> | Y              | F <sup>d</sup> |
| LWH    | 477              | M      | M              | M              | I <sup>d</sup> | M              |
|        | 480              | G      | G              | G              | G              | G              |
| CTL    | 525              | R      | R              | R              | R              | R              |
|        | 526              | N      | N              | N              | N              | N              |
|        | 527              | C      | C              | C              | C              | C              |
|        | 528              | L      | L              | L              | L              | L              |
| AVL    | 539              | D      | D              | D              | D              | D              |
|        | 542 <sup>c</sup> | L      | M <sup>d</sup> | M <sup>d</sup> | M <sup>d</sup> | M <sup>d</sup> |

B4, Beta strand 4; BAC, Beta4-alphaC connector; GRL, glycine rich loop; UPH, upper hinge; LWH, lower hinge; AVL, activation loop; CTL, Catalytic loop. <sup>a</sup> Gatekeeper residue. <sup>b</sup> Catalytic Lysine. <sup>c</sup> Residues that comprise R-spine. <sup>d</sup> Differences in sequence from BTK sequence.

The co-crystallography structure revealed 20 residues within 3 Å of compound **45**, and alignment of the sequences for the Tec family members identified two regions (UPH and AVL) which

are shared to other Tec family members. For example, within the activation loop (AVL region), residue 542 is a leucine in BTK while it is a conserved methionine in TEC, TXK, BMX and ITK. And in the hinge region (UPH) shown to be important for binding to BTK, residue 474 is Thr for BTK and BMX versus a Phenylalanine for TEC, TXK and ITK. Although ITK contains a bulky hydrophobic Phenylalanine 474 gatekeeper compared to the polar conserved Threonine gatekeeper in the other TEC family members, this difference did not impact the overall selectivity for ITK versus BTK. Based on the analysis of the structural data we postulated that differences in the sequence homology within TEC family members could be utilized as a strategy for improving selectivity. Thus, a series of hybrid analogs were designed to interrogate the SAR in both the AVL and the UPH region of the protein.

Table 5. Summary of the *in vitro* biological potency as determined in the enzymatic and cellular assays and the selectivity against the TEC family members.

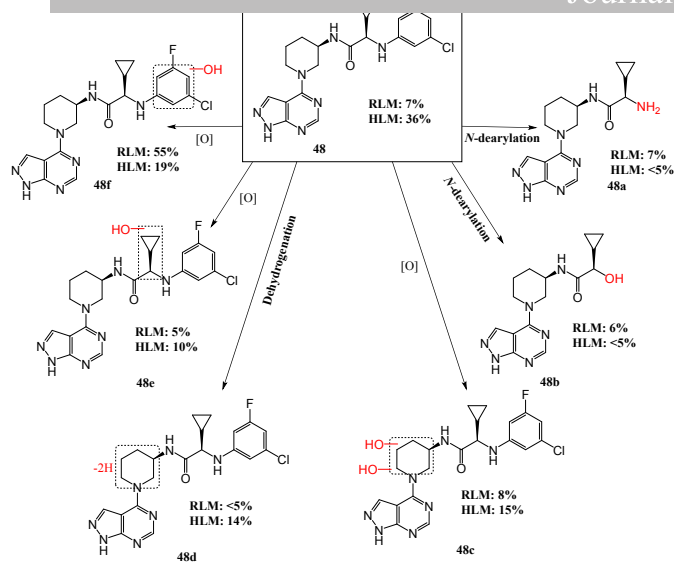


| Cmpd #    | X  | R <sub>1</sub> | R <sub>2</sub>  | BTK IC <sub>50</sub> (μM) <sup>a</sup> | B Cell IC <sub>50</sub> (μM) <sup>b</sup> | BTK, TEC, ITK, TXK, BMX K <sub>d</sub> (μM) <sup>c</sup> | LLE |
|-----------|----|----------------|-----------------|--|---|--|-----|
| <b>41</b> | CH | Cl             | Cl              | 0.012                                  | 0.4                                       | 0.005, 0.05, 0.02, 0.9, 3.8                              | 3.1 |
| <b>45</b> | CH | Cl             | F               | 0.01                                   | 0.34                                      | 0.003, 0.03, 0.02, 0.85, 3.5                             | 3.5 |
| <b>46</b> | CH | Cl             | CF <sub>3</sub> | 0.034                                  | 1.7                                       | 0.04, 0.04, 0.04, 1.6, 3.1                               | 2.3 |
| <b>47</b> | N  | Cl             | Cl              | 0.011                                  | 0.19                                      | 0.006, -, 0.09, 2.5, 7.2                                 | 3.6 |
| <b>48</b> | N  | Cl             | F               | 0.011                                  | 0.2                                       | 0.009, 0.05, 0.19, 5.7, >10                              | 4.2 |
| <b>49</b> | N  | Cl             | CF <sub>3</sub> | 0.057                                  | 0.82                                      | 0.014, 0.07, 0.03, 3.6, 5.6                              | 2.4 |

<sup>a</sup>IC<sub>50</sub> values were determined using non-phosphorylated BTK protein in a FRET assay. <sup>b</sup>IC<sub>50</sub> for B-cell proliferation were measured with peripheral blood mononuclear cells (PBMC's). <sup>c</sup>K<sub>d</sub> were determined in DiscoverX<sup>®</sup> KINOMEScan<sup>™</sup> assays.

Introducing the pyrazolopyrimidine hinge binder led to an improvement in the cellular potency and LLE while affording modest selectivity versus other TEC family members such as ITK, TXK and BMX, but unfortunately, the lead compounds **47** and **48** exhibited low metabolic stability in both the *in vitro* HLM and RLM assays (CL %Q<sub>H</sub> = > 90%).

clearance when dosed IV in a rat PK study.



RLM: rat liver microsomes, HLM: human liver microsomes

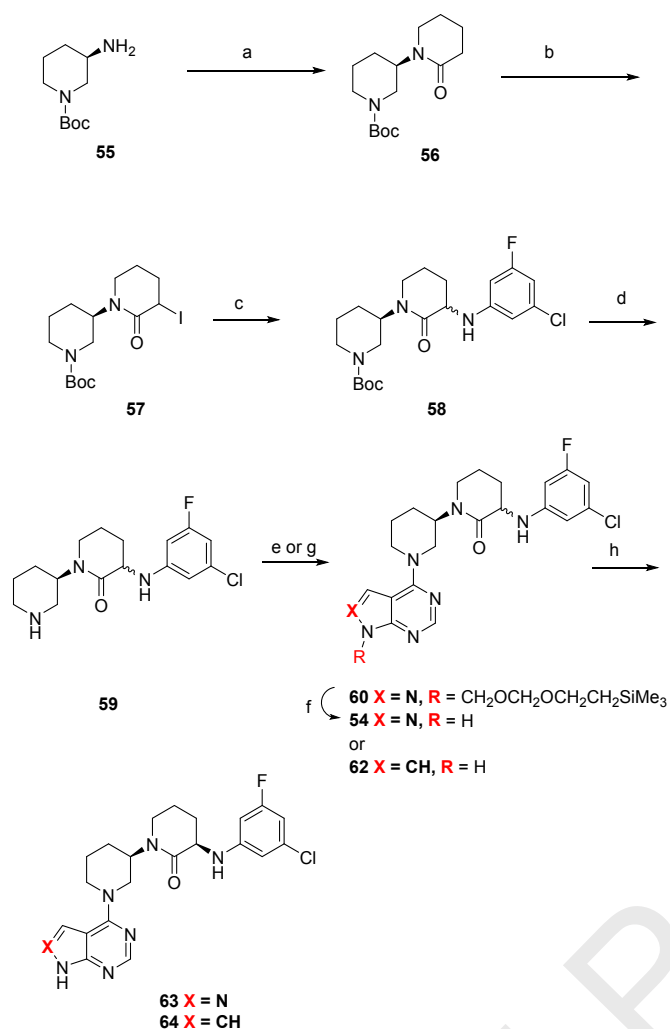
Fig. 5. *In vitro* Met ID profile for compound **48** incubated with human and rat liver microsomes.

The lack of hydrolysis metabolism of carboxamide **48** in *in vitro* in human and rat liver microsome and in rat hepatocytes suggested that hydrolytic enzymes such as amidases were not involved in metabolism of **48**. The major pathways of metabolism identified for compound **48** were *via* oxidation of the piperidine moiety (**48c**), the cyclopropyl moiety (**48e**), and the distal aryl (**48a**, **48f**), in addition to *N*-dearylation at the glycine alpha carbon to afford **48b**. It appeared that introducing the alpha substituent on the glycine linker resulted in the switch of major metabolism to two new sites, including the piperidine motif (**48c** and **48d**) and enhanced metabolism at the distal aryl (**48a** and **48f**). To further interrogate the potential for soft spot switching, a series of analogs were designed to potentially block metabolism of the piperidine and alpha-amino amide linker by introducing deactivating substituents or conformational constraints within the molecule.

The BTK co-crystal structure suggested that introducing a methyl substituent on the amide nitrogen or at the 4-position of the piperidine ring may help improve the potency *via* interacting with the p-loop while introducing steric constraints which could block metabolism in this region of the molecule. Alkylating the amide linker with a methyl group led to a modest improvement in cellular potency but unfortunately **50** demonstrated high *in vitro* and *in vivo* clearance (rat IV CL %Q<sub>H</sub> = >90%). Substituting the piperidine at the 4 position with either a methyl or the trifluoromethyl moiety resulted in an improvement in biochemical and cellular potency as predicted based on the co-crystal structure but again both analogs exhibited high *in vivo* clearance (rat IV CL %Q<sub>H</sub> = >90%). We speculated that introducing conformational rigidity *via* the formation of the 5,6 fused saturated ring system or cyclizing the amide linker as a  $\gamma$ -lactam may improve the *in vivo* clearance while maintaining the potency. Thus, replacing the piperidine moiety with the novel 6,5-diazabicyclic moiety afforded **53** which again was shown to exhibit good cellular potency but poor *in vitro* and *in vivo* metabolic stability (rat IV CL %Q<sub>H</sub> = >90%). Fortunately, it was discovered that the  $\gamma$ -lactam **54**, which had reasonable biochemical potency (Btk IC<sub>50</sub> = 0.015  $\mu$ M), also demonstrated moderate to low *in vivo* clearance (rat IV CL %Q<sub>H</sub> = 32, Table 6) when dosed IV at 0.25 mg/kg in 40% NMP as a 1:1 mixture of diastereomers in a rat PK study.

| Cmpd #    | R | BTK IC <sub>50</sub> ( $\mu$ M) <sup>a</sup> | B Cell IC <sub>50</sub> ( $\mu$ M) <sup>b</sup> | Rat IV CL %Q <sub>H</sub> <sup>c</sup> |
|-----------|---|--|---|--|
| <b>50</b> |   | 0.009  | 0.1   | >90                                    |
| <b>51</b> |   | 0.004  | 0.018   | >90                                    |
| <b>52</b> |   | 0.005  | 0.058   | >90                                    |
| <b>53</b> |   | 0.001  | 0.023   | >90                                    |
| <b>54</b> |   | 0.015  | 1.14  | 48                                     |

<sup>a</sup>IC<sub>50</sub> values were determined using non-phosphorylated BTK protein in a FRET assay. <sup>b</sup>IC<sub>50</sub> for B-cell proliferation were measured with peripheral blood mononuclear cells (PBMC's). <sup>c</sup>Predicted hepatic oxidative clearance was measured in rat liver microsomal (LM) fraction, Q<sub>H</sub> hepatic blood flow (portal vein plus hepatic artery).



**Scheme 3. Reagents and conditions:** (a) i. C<sub>5</sub>H<sub>8</sub>OBrCl, Et<sub>3</sub>N, CH<sub>2</sub>Cl<sub>2</sub>, 0 °C, 3 hr 80% yield; ii. NaH, THF, 0 °C to 70 °C, 3 hr, 90% yield; (b) TMEDA, TMSCl, Ph-CH<sub>3</sub>, I<sub>2</sub>, 0 °C to rt, 18 hr, 60% yield; (c) 3-Chloro-5-fluoroaniline, NaH, THF, 60 °C, 3 hr, 45% yield; (d) TFA, CH<sub>2</sub>Cl<sub>2</sub>, rt, 2 hr, 91% yield; (e) i. C<sub>12</sub>H<sub>19</sub>ClN<sub>4</sub>O<sub>2</sub>Si, *n*-butanol, Et<sub>3</sub>N, 80 °C, 2 hr, 85% yield; (f) i. HCl, 1,4-dioxane, 70 °C, 1 hr, 95% yield; (g) i. C<sub>4</sub>H<sub>4</sub>ClN<sub>3</sub>, *n*-butanol, Et<sub>3</sub>N, 80 °C, 2 hr, 79% yield; (h) Preparative chiral SFC separation.

The synthesis of chiral cyclic amide **63** began with acylation of *tert*-butyl piperidin-3-ylcarbamate **55** upon treatment with 5-bromovaleryl chloride, which was subsequently treated with NaH in DMF at rt for 24 hr to facilitate cyclization to **56** in a 72% yield. Amination at the  $\alpha$ -position of the  $\gamma$ -lactam was accomplished in a two-step sequence, beginning with treatment of **56** with TMEDA, TMSCl and iodine to afford intermediate **57** which was subsequently reacted with 3-chloro-5-fluoroaniline under basic conditions to afford **58** as a 1:1 mixture of diastereomers in an overall 27% yield. Deprotection of the Boc group with HCl followed by *N*-arylation upon treatment of the SEM protected 4-chloro-pyrazolopyrimidine under mild basic conditions, followed by deprotection afforded **61** which was separated using SFC to afford the enantiomer **63**.

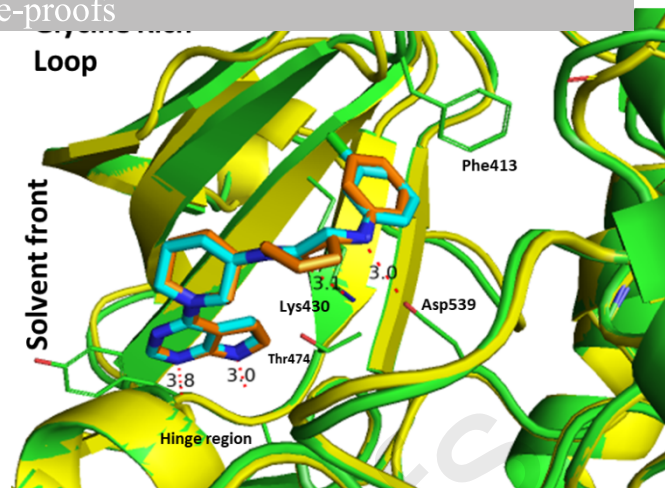


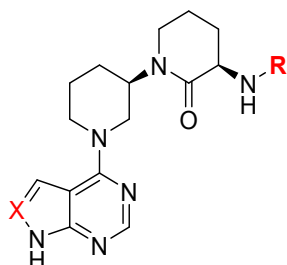
**Fig. 6** An overlay of the crystal structures of compounds **21** (blue/green) and **65** (brown/yellow) bound to BTK kinase.

With a viable synthesis in hand to enable further optimization of the cyclic amide series, attention switched to establishing the SAR which would confer good biochemical and cellular potency, kinase selectivity, and reduced *in vivo* clearance. An overlay of the co-crystal structures for **21** and **65** (racemic des-halo analog, BTK IC<sub>50</sub> = 0.19  $\mu$ M) indicated that the new cyclic amide series exhibited a binding pose where the  $\alpha$  amino-lactam moiety maintained the unique bi-dentate HBD/HBD interactions with the catalytic Lys-430 and Asp-539 while orienting the distal phenyl ring to bind in a putative hydrophobic pocket similar to the binding pose observed with the glycine series (Figure 6). Based on the structure, a series of analogs were synthesized as single enantiomers designed to re-explore the distal phenyl moiety since based on the prior SAR (table 4) this region of the molecule was shown to be very amenable for modulating the biochemical potency, kinase selectivity and physicochemical properties.

Both the cyclic amide and glycine series exhibited similar SAR trends with respect to modification on the distal aryl motif. For example, compounds **63** and **66** containing the 3-fluoro-5-chlorophenyl and the 3,5-dichlorophenyl moieties demonstrated biochemical potencies within < 2 fold of **42** and **43**, although the biochemical potency observed within the lactam resulted in a significant loss in cellular potency (PBMC CD69 IC<sub>50</sub> = 1.2  $\mu$ M (**63**)) compared to the acyclic series (PBMC CD69 IC<sub>50</sub> = 0.09  $\mu$ M (**47**)). This result was attributed to the increase in the lipophilicity (**63** Log D = 4.6 *versus* **47** Log D = 4) resulting in an increase in plasma protein binding (% Fu = 1 (**63**) *versus* % Fu = 6 (**47**)) and a decrease in the kinetic solubility at pH 6.8 (<1  $\mu$ g/mL *versus* 7  $\mu$ g/mL respectively). Since the lead compound **54** had been dosed *in vivo* as a mixture of diastereomers, it was necessary to first determine if the single enantiomer would exhibit similar *in vivo* stability compared to the diastereomeric mixture. Unfortunately, when **63** was dosed IV in a rat PK study, the enantiomer demonstrated higher *in vivo* plasma clearance (**63**, rat IV CL %Q<sub>H</sub> = 70) compared to **54** (rat IV CL %Q<sub>H</sub> = 48 as a 1:1 mixture of diastereomers), thus reiterating the need to complete the PK studies using chiral material. In addition, switching the distal phenyl to the 3,5-dichlorophenyl moiety afford **66** with high clearance (rat IV CL %Q<sub>H</sub> = >100) when dosed as an IV cassette (0.25 mg/kg, 40% NMP) in Sprague Dawley rats. The addition of a fluoro atom at the para position of the distal phenyl **67** and **68** improved the *in vivo* clearance compared to **63** and **65**. This finding was consistent with the Met ID studies as the 4 position had been identified as a potential site for metabolism (Schemes 3 and 5) but unfortunately, these analogs were less potent in the

pyrazolo-pyrimidine to the pyrrolo-pyrimidine afforded **64** with moderate *in vivo* clearance ( $CL \%Q_H = 50$ ), adequate bioavailability ( $\%F = 48$ ) when dosed at 5 mg/kg as an amorphous solid as suspension formulation in carboxymethyl cellulose (CMC)/Tween, good biochemical potency (BTK  $IC_{50} = 0.004 \mu M$ ) and cellular activity (PBMC CD69  $IC_{50} = 0.63 \mu M$ ).

**Table 7.** Summary of the *in vitro* biological potency and *in vivo* clearance when single enantiomers are dosed IV in a rat PK study.

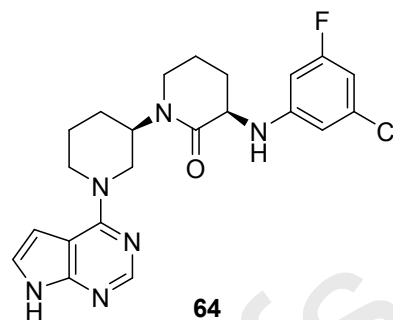


| Cmpd # | R | X  | Btk $IC_{50}$ ( $\mu M$ ) <sup>a</sup> | B cell $IC_{50}$ ( $\mu M$ ) <sup>b</sup> | Rat IV CL $\%Q_H$ <sup>c</sup> | LLE |
|--------|---|----|--|---|--------------------------------|-----|
| 63     |   | N  | 0.010                                  | 1.95                                      | 70                             | 3.8 |
| 66     |   | N  | 0.008                                  | 1.62                                      | >90                            | 3.9 |
| 67     |   | N  | 0.053                                  | 4.85                                      | 28                             | 3.5 |
| 68     |   | N  | 0.018                                  | 3.39                                      | 18                             | 3.3 |
| 64     |   | CH | 0.004                                  | 0.630                                     | 53                             | 4.3 |

<sup>a</sup> $IC_{50}$  values were determined using non-phosphorylated BTK protein in a FRET assay. <sup>b</sup> $IC_{50}$  for B-cell proliferation were measured with peripheral blood mononuclear cells (PBMC's). <sup>c</sup> Predicted hepatic oxidative clearance was measured in rat liver microsomal (LM) fraction,  $Q_H$  hepatic blood flow (portal vein plus hepatic artery).

In addition to the favorable biological and *in vivo* pharmacokinetic properties, compound **64** inhibited 18/459 kinases by >80% when tested at 0.7  $\mu M$  (100-fold over the BTK  $K_d$ ) and modest BTK selectivity *versus* other members of the Tec family members (Tec  $K_d = 0.013 \mu M$ , ITK  $K_d = 0.082 \mu M$ , TXK  $K_d = 1.6 \mu M$ , BMX  $K_d = 2.7 \mu M$ ) when tested at DiscoverX. Profiling of the ADME properties indicated that **64** exhibited weak CYP inhibition toward 3A4 (CYP  $IC_{50} = 1.3 \mu M$ ) only when tested using testosterone, and no activity against other isoforms ( $IC_{50} = >10 \mu M$ ). Compound **64** showed good intrinsic permeability with no efflux and pH dependent solubility (kinetic pH 3 and 6.8 >50  $\mu g/mL$  & <1  $\mu g/mL$ ). Applying a minimal PBP model, the human PK properties for **64** were simulated with a predicted CL of 1.4 mL/min/Kg (from liver microsomal stability),  $V_{ss}$  (from physicochemical properties) of 1.28 L/Kg, and an estimated  $k_a$  of 0.9/hr<sup>-1</sup> (from observed  $k_a$  in preclinical species for this series).

**Table 8:** Summary of biological, ADMR and physical chemical properties for compound **64**.



| Assay  | Compd 64                      |
|--|-------------------------------|
| <b>Physical-chemical properties:</b> MW, Log D, PSA, LLE <sup>26</sup>               | 442, 4.5, 77, 4.3             |
| <b>Biochemical potency:</b> BTK $IC_{50} \mu M^a$                                    | 0.004                         |
| <b>Cellular potency:</b> B-cell proliferation anti-IgM+IL-4 $IC_{50} \mu M^b$        | 0.63                          |
| <b>Selectivity against TEC family members:</b> BTK, ITK, TEC, TXK, BMX $K_D \mu M^c$ | 0.007, 0.013, 0.083, 1.6, 2.7 |
| <b>Aqueous kinetic solubility:</b> $\mu g/mL$ at pH 6.8 and 1.5 <sup>d</sup>         | 1, >40                        |
| <b>Permeability:</b> Caco-2 A-B Papp ( $10^{-6}$ cm/sec), efflux ratio <sup>e</sup>  | 28, 1.4                       |
| <b>Metabolic stability:</b> Human, rat <i>in vitro</i> liver microsomal CL $\%Q_H^f$ | 3.6, 18                       |
| <b>Plasma protein binding:</b> $\%Fu$ human, rat <sup>g</sup>                        | 1.1, 1.9                      |
| <b>Rat<sup>h</sup> PK</b>  |                               |
| IV (dose 1 mg/kg), CL (ml/min/kg), CL $\%Q_H$ $V_{ss}$ (L/kg), $T_{1/2}$ (hr)        | 29, 55, 1.6, 0.8              |
| PO (dose 5 mg/kg suspension), $AUC_{inf}$ (hr*mg/mL), $T_{max}$ (hr), F (%)          | 632, 0.5, 48%                 |

<sup>a</sup> $IC_{50}$  values were determined using non-phosphorylated protein in a biochemical assay. <sup>b</sup> $IC_{50}$  for B-cell proliferation were measured with peripheral blood mononuclear cells (PBMC's). <sup>c</sup> $K_d$  were determined in DiscoverX® KINOMEscan™ assays. <sup>d</sup>Kinetic solubility was measured using Analiza® miniaturized shake flask assay. <sup>e</sup>Trans epithelial transport across Caco-2/TC-7 monolayers. <sup>f</sup>Predicted hepatic oxidative clearance was measured in liver microsomal fraction and corrected for microsomal binding ( $\%Q_H$  hepatic blood flow (portal vein plus hepatic artery)). <sup>g</sup>Plasma protein binding (PPB) **50** at a concentration of 2  $\mu M$  was assessed for rat, and human plasma, via rapid equilibrium dialysis (RED). <sup>h</sup>PK studies were conducted in Sprague Dawley rats dosing IV as a solution in 40% NMP and PO as a suspension in carboxymethyl cellulose (CMC)/Tween.

## Conclusion

Herein, we describe the use of structure-based design to identify BTK inhibitors which were optimized focusing on improving the physical chemical properties to increase potency, kinome selectivity, and *in vivo* plasma stability leading to the discovery of a novel cyclic lactam series. The most advanced molecule from the

biological and ADME properties to transition into lead optimization, ultimately leading to the discovery of vecabrutinib, which was taken into clinical to evaluate as a treatment for patients diagnosed with relapsed/refractory chronic lymphocytic leukemia (CLL).

**General.** All reagents and solvents were purchased from commercial sources and were used without further purification. Reaction progress was monitored by LCMS. Flash chromatography was performed with Isco Combiflash Companion system using pre-packed silica gel columns. <sup>1</sup>H NMR spectra were recorded at 400 MHz and 600 MHz using a Bruker AVANCE III spectrometer with a BBFO probe. Compound purities were estimated by reversed-phase C18 HPLC, and SFC with a UV detector at 214 and 254 nm, and the major peak area of each tested compound was ≥95% of the combined total peak area.

**tert-Butyl (R)-2-oxo-[1,3'-bipiperidine]-1'-carboxylate (56).** To a solution of *tert*-butyl (R)-3-aminopiperidine-1-carboxylate (20.0 g, 100 mmol) and Et<sub>3</sub>N (20.2 g, 200 mmol) in CH<sub>2</sub>Cl<sub>2</sub> (200 mL) was added 5-bromopentanoyl chloride (23.8 g, 120 mmol) at 0 °C. The mixture was stirred at rt for 3 hr and concentrated *in vacuo*, diluted with water and extracted with EtOAc (200 mL X 3). The combined organic layers were dried (Na<sub>2</sub>SO<sub>4</sub>), filtered and concentrated *in vacuo* to afford an oil (25.0 g, 68.5 mmol) which was dissolved in THF (200 mL) and treated with NaH (4.9 g, 205 mmol) at 0 °C. The mixture was stirred at 70 °C for 3 hr under N<sub>2</sub>, quenched with water, extracted with EtOAc (200 mL X 3), the organic layer were dried (Na<sub>2</sub>SO<sub>4</sub>), filtered and concentrated *in vacuo* to afford a residue which was purified by silica gel column (Petroleum ether: EtOAc = 1:9 (v/v)) to afford *tert*-butyl (R)-2-oxo-[1,3'-bipiperidine]-1'-carboxylate **57** (18.0 g, 90%) as yellow oil. <sup>1</sup>H NMR (400 MHz, CDCl<sub>3</sub>) δ 3.25 (m, 1H) 3.18 (m, 2H), 2.82 (t, *J* = 11.8, 11.8 Hz, 1H), 2.81 (m, 1H), 2.57 (br s, 1H), 2.41 (br s, 2H), 1.77 (br s, 4H), 1.64 (m, 6H), 1.45 (s, 9H); <sup>13</sup>C NMR (400 MHz, CDCl<sub>3</sub>) δ 20.74, 23.37, 27.32, 28.42, 32.63, 43.28, 79.80, 154.83, 169.72; ESI-MS (*m/z*): 227.3, calcd for [M+H]<sup>+</sup> - *tert*Butyl C<sub>11</sub>H<sub>18</sub>N<sub>2</sub>O<sub>3</sub>: 227.3.

**tert-Butyl (3'R)-3-((3-chloro-5-fluorophenyl)amino)-2-oxo-[1,3'-bipiperidine]-1'-carboxylate (58).** To a solution of **56** (4.5 g, 16 mmol) in PhCH<sub>3</sub> (80 mL) was added *N*<sub>1</sub>,*N*<sub>1</sub>,*N*<sub>2</sub>,*N*<sub>2</sub>-tetramethylethane-1,2-diamine (8.7 g, 97.5 mmol) and TMSCl (7.0 g, 65 mmol) at 0 °C and allowed to stir for 6 hr, followed by the addition of I<sub>2</sub> (8.0 g, 32.5 mmol) and stirred at rt overnight under N<sub>2</sub>. The mixture was quenched with water, extracted with EtOAc (100 mL X 3) and the combined organic layers were dried (Na<sub>2</sub>SO<sub>4</sub>), filtered and concentrated *in vacuo* to give *tert*-butyl (3'R)-3-iodo-2-oxo-[1,3'-bipiperidine]-1'-carboxylate **57** (4.0 g, 60 %) as yellow solid. Intermediate **57** (4.0 g, 10 mmol) was dissolved in THF (20 mL) and added slowly at rt to a solution of 3-chloro-5-fluoroaniline (2.2 g, 15 mmol) and NaH (0.36 g, 15 mmol) in THF (40 mL). The mixture was heated at 60 °C for 3 hr under N<sub>2</sub>, quenched with NH<sub>4</sub>Cl, extracted with EtOAc (100 mL X 3), dried (Na<sub>2</sub>SO<sub>4</sub>), filtered and concentrated *in vacuo* to afford a residue which was purified by silica gel column (Petroleum ether: EtOAc = 1:1 (v/v)) to give *tert*-Butyl (3'R)-3-iodo-2-oxo-[1,3'-bipiperidine]-1'-carboxylate **58** as yellow oil (1.8 g, 45%). <sup>1</sup>H NMR (400 MHz, CDCl<sub>3</sub>) δ 6.34 (br d, 8.2 Hz, 1H), 6.39 (br s, 1H), 6.22 (dt, *J* = 11.1, 2.0, 2.0 Hz, 1H), 5.23 (s, 1H), 3.78 (br m, 1H), 3.32 (ddd, *J* = 10.2, 9.8, 4.9 Hz, 2H), 2.88 – 2.76 (m, 1H), 2.47 (br s, 1H), 1.98 – 1.86 (m, 2H), 1.83 (br m, 1H), 1.72 (br d, *J* = 11.8 Hz, 1H), 1.65 (br m, 1H), 1.60 (s, 3H), 1.46 (br d, 9H); <sup>13</sup>C NMR (400 MHz, CDCl<sub>3</sub>) δ 20.70, 21.07, 26.44,

109.09, 135.44, 149.37, 154.71, 154.76, 162.54, 164.98, 169.95; LCMS (ESI): *m/z* 370.1 (M+H)<sup>+</sup> - *tert*Butyl C<sub>17</sub>H<sub>21</sub>N<sub>3</sub>ClFO<sub>3</sub>: 370.1.

**(3'R)-3-((3-chloro-5-fluorophenyl)amino)-[1,3'-bipiperidin]-2-one (59).** To solution of **58** (1.8 g, 4.2 mmol) in CH<sub>2</sub>Cl<sub>2</sub> (20 mL) was added TFA (3 mL) and was stirred at rt 2 hr. The reaction solution was adjusted to pH = 7 - 8 with NaHCO<sub>3</sub>, extracted with EtOAc (50 mL X 3), dried (Na<sub>2</sub>SO<sub>4</sub>), filtered and concentrated *in vacuo* to afford **59** as colorless oil (1.5 g, 91%). <sup>1</sup>H NMR (500 MHz, CD<sub>3</sub>OD-*d*<sub>4</sub>) δ 6.49 (s, 1H), 6.35 (d, *J* = 1.22 Hz, 1H), 6.32-6.34 (m, 2H), 4.31-4.41 (m, 1H), 4.01 (dd, *J* = 6.64, 1.07 Hz, 1H), 3.35-3.42 (m, 1H), 3.27-3.34 (m, 1H), 2.92 (br t, *J* = 11.60 Hz, 2H), 2.68 (dt, *J* = 4.58, 11.75 Hz, 1H), 2.40-2.50 (m, 1H), 2.17-2.27 (m, 1H), 1.86-1.93 (m, 5H), 1.70-1.76 (m, 2H), 1.54-1.69 (m, 2H). <sup>13</sup>C NMR (126 MHz, CD<sub>3</sub>OD-*d*<sub>4</sub>) δ 172.4, 166.3, 164.4, 152.2, 136.4, 110.1, 104.6, 99.2, 54.7, 53.5, 46.4, 43.2, 28.0, 27.4, 22.0; LCMS (ESI): *m/z* 326.2 (M+H)<sup>+</sup>.

**(3'R)-3-((3-Chloro-5-fluorophenyl)amino)-1'-((2-(trimethylsilyl)ethoxy)methyl)-1*H*-pyrazolo[3,4-*d*]pyrimidin-4-yl)-[1,3'-bipiperidin]-2-one (60).** A solution of **59** (1.5 g, 4.6 mmol), 4-chloro-1-((2-(trimethylsilyl)ethoxy)methyl)-1*H*-pyrazolo[3,4-*d*]pyrimidine (1.3 g, 4.6 mmol), Et<sub>3</sub>N (0.9 g, 9 mmol) in *n*-butanol (20 mL) was heated to 80 °C for 2 hr, the mixture was allowed to cool to rt diluted with water and extracted with EtOAc (20 mL X 3), the combined organic layers were dried (Na<sub>2</sub>SO<sub>4</sub>), filtered and concentrated *in vacuo* to afford a residue which was purified silica gel column (Petroleum ether: EtOAc = 1: 9 (v/v)) to give (3'R)-3-((3-Chloro-5-fluorophenyl)amino)-1'-((2-(trimethylsilyl)ethoxy)methyl)-1*H*-pyrazolo[3,4-*d*]pyrimidin-4-yl)-[1,3'-bipiperidin]-2-one **69** (1.8 g, yield: 85%) as white solid. <sup>1</sup>H NMR (500 MHz, CD<sub>3</sub>OD-*d*<sub>4</sub>) δ 8.27 (s, 1H), 8.26 (d, *J* = 1.22 Hz, 1H), 6.49 (s, 1H), 6.28-6.37 (m, 2H), 5.67 (s, 2H), 4.86 (s, 2H), 4.63-4.81 (m, 1H), 4.31-4.46 (m, 1H), 4.06 (ddd, *J* = 6.41, 10.53, 12.36 Hz, 1H), 3.63 (t, *J* = 8.24 Hz, 2H), 3.39-3.53 (m, 2H), 3.32-3.37 (m, 1H), 3.10 (br s, 1H), 2.18-2.31 (m, 1H), 1.86-2.06 (m, 5H), 1.62-1.78 (m, 2H), 0.83-0.92 (m, 2H), -0.07 (d, *J* = 1.83 Hz, 9H); <sup>13</sup>C NMR (126 MHz, CD<sub>3</sub>OD-*d*<sub>4</sub>) δ 172.7, 166.3, 164.4, 158.3, 156.5, 156.1, 152.2, 136.4, 135.7, 110.0, 104.6, 101.9, 99.2, 76.2, 68.1, 54.8, 52.9, 52.7, 43.7, 28.5, 28.0, 25.8, 22.1, 18.7, -1.3; LCMS (ESI): *m/z* 574.1 (M+H)<sup>+</sup>; C<sub>27</sub>H<sub>37</sub>N<sub>7</sub>ClFO<sub>2</sub>Si: 574.1.

**(3'R)-3-((3-Chloro-5-fluorophenyl)amino)-1'-((1*H*-pyrazolo[3,4-*d*]pyrimidin-4-yl)-[1,3'-bipiperidin]-2-one (54).** To a solution of **60** (1.8 g, 3.1 mmol) in MeOH (15 mL) was added 4 N HCl in 1,4-dioxane (1 mL) and stirred at 70 °C for 1 hr. The reaction extracted with EtOAc (50 mL X 3) and the combined organic layers were dried (Na<sub>2</sub>SO<sub>4</sub>), filtered, concentrated *in vacuo* to afford an oil which was purified silica gel column (Petroleum ether: EtOAc = 1: 9 (v/v)) to give (3'R)-3-((3-Chloro-5-fluorophenyl)amino)-1'-((1*H*-pyrazolo[3,4-*d*]pyrimidin-4-yl)-[1,3'-bipiperidin]-2-one **61** as white solid (1.0 g, yield: 95%). <sup>1</sup>H NMR (500 MHz, CD<sub>3</sub>OD-*d*<sub>4</sub>) δ 8.21 (d, *J* = 3.66 Hz, 2H), 6.45-6.54 (m, 1H), 6.28-6.39 (m, 2H), 4.62-4.82 (m, 2H), 4.31-4.43 (m, 1H), 4.06 (ddd, *J* = 6.10, 10.07, 13.12 Hz, 1H), 3.46 (dtd, *J* = 6.10, 12.17, 17.78 Hz, 2H), 3.35 (br s, 1H), 3.10 (br s, 1H), 2.19-2.29 (m, 1H), 1.88-2.04 (m, 5H), 1.62-1.78 (m, 2H); <sup>13</sup>C NMR (126 MHz, CD<sub>3</sub>OD-*d*<sub>4</sub>) δ 172.7, 166.4, 164.4, 158.4, 156.5, 156.3, 152.2, 136.4, 135.5, 110.0, 104.6, 101.2, 99.2, 54.8, 52.9, 43.8, 28.6, 28.4, 28.0, 25.8, 22.1. LCMS (ESI): *m/z* 444.1 (M+H)<sup>+</sup>; C<sub>21</sub>H<sub>23</sub>ClFN<sub>7</sub>O: 444.1. Anal. Calcd for C<sub>21</sub>H<sub>23</sub>N<sub>7</sub>O<sub>1</sub>Cl<sub>1</sub>F<sub>1</sub> 0.5H<sub>2</sub>O: C, 55.69; H, 5.34; N, 21.65; Found C, 55.65; H, 5.19; N, 21.30.

**pyrrolo[2,3-d]pyrimidin-4-yl)-[1,3'-bipiperidin]-2-one (64).** To a solution of **59** (0.23 g, 6.9 mmol) and 4-chloro-7H-pyrrolo[2,3-d]pyrimidine (0.1 g, 6.9 mmol) in DMF (3.45 mL) was added Hunigs base (0.27 g, 20.7 mmol, 0.36 mL) and stirred at 100 °C for 6 hr. The reaction was diluted with water and extracted with EtOAc (50 mL X 2) and the combined organic layers were dried (Na<sub>2</sub>SO<sub>4</sub>), filtered, concentrated *in vacuo* to afford an oil which was purified silica gel column (Petroleum ether: EtOAc = 1: 9 (v/v)) to give (3'R)-3-((3-Chloro-5-fluorophenyl)amino)-1'-(1H-pyrrolo[3,4-d]pyrimidin-4-yl)-[1,3'-bipiperidin]-2-one **61** as an off white solid (0.24 g, yield: 79%).

The diastereomers were separated via SFC chiral chromatography (CHIRALPAK IB 30x250mm, 5um Method: 40% MeOH w/ 0.1% DEA in CO<sub>2</sub> (flow rate: 100mL/min, ABPR 120bar, MBPR 40psi, column temp 40 deg C) to afford (3R)-3-(3-chloro-5-fluoro-anilino)-1-[(3R)-1-(7H-pyrrolo[2,3-d]pyrimidin-4-yl)-3-piperidyl]piperidin-2-one (96.60 mg, 218.10 umol, 31.58% yield) (Peak 1) and (3S)-3-(3-chloro-5-fluoro-anilino)-1-[(3R)-1-(7H-pyrrolo[2,3-d]pyrimidin-4-yl)-3-piperidyl]piperidin-2-one (0.0706 g, 159.40 umol, 23.08% yield) (Peak 2) as off-white solids. <sup>1</sup>H NMR (500 MHz, CD<sub>3</sub>OD-d<sub>4</sub>) δ 8.12 (s, 1H), 7.08 (d, *J* = 3.66 Hz, 1H), 6.61 (d, *J* = 3.66 Hz, 1H), 6.49 (s, 1H), 6.34 (dd, *J* = 2.14, 3.36 Hz, 1H), 6.32 (d, *J* = 1.83 Hz, 1H), 4.61-4.72 (m, 2H), 4.36-4.46 (m, 1H), 4.02 (dd, *J* = 6.10, 9.77 Hz, 1H), 3.33-3.48 (m, 2H), 3.18 (t, *J* = 11.90 Hz, 1H), 2.95-3.04 (m, 1H), 2.16-2.25 (m, 1H), 1.83-1.98 (m, 5H), 1.62-1.74 (m, 2H). <sup>13</sup>C NMR (126 MHz, CD<sub>3</sub>OD-d<sub>4</sub>) δ 172.6, 166.3, 164.4, 158.4, 152.5, 152.2, 151.7, 136.4, 122.6, 110.1, 104.7, 104.5, 102.7, 99.2, 54.7, 52.9, 47.4, 43.5, 28.8, 28.0, 26.1, 22.0. LCMS (ESI): *m/z* 444.1 (M+H)<sup>+</sup>; C<sub>22</sub>H<sub>24</sub>ClFN<sub>6</sub>O: 443.1. Anal. Calcd for C<sub>22</sub>H<sub>24</sub>N<sub>6</sub>O<sub>1</sub>ClF<sub>1</sub>: C, 59.66; H, 5.46; N, 18.97; Found C, 59.18; H, 5.31; N, 18.70.

**Methods for BTK biochemical activity assay:** Compound inhibition was measured after monitoring the amount of phosphorylation of a fluorescent-labeled polyGAT peptide in the presence of active BTK enzyme (Millipore 14-552), ATP, and an inhibitor. The BTK kinase reaction was performed a black 96-well plate (Corning 3694). For a typical assay, a 24 μL aliquot of a ATP/peptide master mix (final concentration; ATP 10 μM, polyGAT 100 nM) in kinase buffer (10 mM Tris-HCl pH 7.5, 10 mM MgCl<sub>2</sub>, 200 μM Na<sub>3</sub>PO<sub>4</sub>, 5 mM DTT, 0.01% Triton X-100, and 0.2 mg/mL casein) was added to each well. Next, 1 μL of a 4-fold, 40X compound titration in 100% DMSO solvent was added, followed by 15 μL of BTK enzyme mix in 1X kinase buffer (with a final concentration of 0.25 nM). The assay was incubated for 30 minutes then stopped with 28 μL of a 50 mM EDTA solution. Aliquots (5 μL) of the kinase reaction were transferred to a low volume, white 384-well plate (Corning 3674), and 5 μL of a 2X detection buffer (Invitrogen PV3574, with 4 nM Tb-PY20 antibody, Invitrogen PV3552) was added. The plate was covered and incubated for 45 minutes at room temperature. Time resolved fluorescence (TRF) on Molecular Devices M5 plate reader (332 nm excitation; 488 nm emission; 518 nm fluorescein emission) was measured. IC<sub>50</sub> values were calculated using a four-parameter curve fit with 100% enzyme activity determined from the DMSO control and 0% activity from the EDTA control.

**Cell based assay:** Human peripheral blood mononuclear cells (PBMC) were purified from heparinized whole blood using Ficoll-Paque (GE Healthcare Life Sciences, Pittsburgh, PA) density gradient centrifugation. B cells were then enriched from the isolated PBMC using the Human B Cell Isolation Kit II (Miltenyi Biotec, Bergisch Gladbach, Germany) according to the manufacturer's instruction. A minimum purity of B cells (98%) was confirmed by flow cytometry with an antibody against human CD19 (BD Biosciences, Franklin Lakes, NJ). Purified B cells (5 x

with serially diluted BTK inhibitors as indicated in 96-well round bottom plates (Corning, Corning, NY) for 30 min at 37 °C. Following incubation of B cells with BTK inhibitors, cells were stimulated for 3 days with F(ab')<sub>2</sub> goat anti-human IgM antibody (10 μg/mL; Jackson ImmunoResearch, West Grove, PA) and recombinant human IL-4 (X μg/mL; R&D Systems, City, State). At the end of day 3, an equal volume of CellTiter-Glo® Reagent (Promega, Madison, WI) was added to the cell culture and the contents were mixed on an orbital shaker for 2 min at room temperature. The samples were then rested for an additional 10 min at RT and the emitted luminescent signals were measured with a SpectraMax luminometer (Molecular Devices, Sunnyvale, CA). The luminescence relative units (RLU) from the inhibitor-treated samples were then graphed versus log<sub>10</sub> inhibitor concentration in GraphPad Prism and the IC<sub>50</sub> value was determined.

**Methods for Caco-2 permeability assay:** Caco-2 cell monolayers were grown to confluence on microporous polyethylene membranes in 24-well BD Falcon™ insert plates. The permeability assay buffer was HBSS containing 25 mM HEPES at pH of 7.4. The buffer in the receiver chamber also contained 1% bovine serum albumin. DMSO stock solutions were prepared at 5 μM in assay buffer from 10 mM stock solution, and added to the apical side and basolateral side. Cells were incubated at 37 °C with 5% CO<sub>2</sub> in a humidified incubator. Samples were collected from the donor chambers at 0 and 120 minutes, and receiver chambers at 120 minutes. After samples were collected, 100 μM lucifer yellow was added to all apical chambers, and fresh buffer was added to the basolateral chambers. The permeability of lucifer yellow was measured for each monolayer for 60 minutes to ensure the integrity of the cell monolayers during the test compound flux period. The apparent permeability coefficient, P<sub>app</sub>, was calculated as follows:

$$P_{app} = (dCr / dt) \times V_r / (A \times CE)$$

Where *dCr / dt* is the permeation rate of cumulative concentration in the receiver compartment *versus* time in μM s<sup>-1</sup>, V<sub>r</sub> is the volume of the receiver compartment in cm<sup>3</sup>, A is the area of the insert (0.31 cm<sup>2</sup> for 24-well insert), CE is the calculated experimental concentration (Time = 0) of the dosing solution in μM, determined via LC/MSMS.

## Acknowledgments

The team is grateful for Biogen Inc. and Sunesis Pharmaceuticals, Inc. for providing financial support to this work.

## Appendix A. Supplementary Material

Supplementary data to this article can be found online at

## References and notes

- Berg, L. J.; Finkelstein, L. D.; Lucas, J. A.; Schwartzberg, P. L., Tec family kinases in T lymphocyte development and function. *Annu Rev Immunol* **2005**, *23*, 549-600.
- Vetrie D, Vorechovsky I, Sideras P, Holland J, Davies A, Flinter F, Hammarstrom L, Kinnon C, Levinsky R, Bobrow M, et al. The gene involved in X-linked agammaglobulinemia is a member of the src family of protein-tyrosine kinases. *Nature*. **1993**, *361* (6409), 226-233.
- Tsukada S, Saffran DC, Rawlings DJ, Parolini O, Allen RC, Klisak I, Sparkes RS, Kubagawa H, Mohandas T, Quan S, et al. Deficient expression of a B cell cytoplasmic tyrosine kinase in human X-linked agammaglobulinemia. *Cell*. **1993**, *72* (2), 279-290.

- B cells in rheumatoid arthritis: from pathogenic players to disease biomarkers. *Biomed Res Int* **2014**, *2014*, 681678.
5. Franciotta, D.; Salvetti, M.; Lolli, F.; Serafini, B.; Aloisi, F., B cells and multiple sclerosis. *Lancet Neurol* **2008**, *7* (9), 852-8.
  6. Montalban, X.; Arnold, D. L.; Weber, M. S.; Staikov, I.; Piasecka-Stryczynska, K.; Willmer, J.; Martin, E. C.; Dangond, F.; Syed, S.; Wolinsky, J. S.; Evobrutinib Phase 2 Study, G., Placebo-Controlled Trial of an Oral BTK Inhibitor in Multiple Sclerosis. *N Engl J Med* **2019**, *380* (25), 2406-2417.
  - 7.urger, J. A., Bruton Tyrosine Kinase Inhibitors: Present and Future. *Cancer J* **2019**, *25* (6), 386-393.
  8. Honigberg, L. A.; Smith, A. M.; Sirisawad, M.; Verner, E.; Loury, D.; Chang, B.; Li, S.; Pan, Z.; Thamm, D. H.; Miller, R. A.; Buggy, J. J., The Bruton tyrosine kinase inhibitor PCI-32765 blocks B-cell activation and is efficacious in models of autoimmune disease and B-cell malignancy. *Proc Natl Acad Sci U S A* **2010**, *107* (29), 13075-80.
  9. Wang, M.; Rule, S.; Zinzani, P. L.; Goy, A.; Casasnovas, O.; Smith, S. D.; Damaj, G.; Doorduijn, J. K.; Lamy, T.; Morschhauser, F.; Panizo, C.; Shah, B.; Davies, A.; Eek, R.; Dupuis, J.; Jacobsen, E.; Kater, A. P.; Le Gouill, S.; Oberic, L.; Robak, T.; Jain, P.; Frigault, M. M.; Izumi, R.; Nguyen, D.; Patel, P.; Yin, M.; Dlugosz-Danecka, M., Durable response with single-agent acalabrutinib in patients with relapsed or refractory mantle cell lymphoma. *Leukemia* **2019**, *33* (11), 2762-2766.
  10. Syed, Y. Y., Zanubrutinib: First Approval. *Drugs* **2020**, *80* (1), 91-97.
  11. Woyach, J. A.; Furman, R. R.; Liu, T. M.; Ozer, H. G.; Zapatka, M.; Ruppert, A. S.; Xue, L.; Li, D. H.; Steggerda, S. M.; Versele, M.; Dave, S. S.; Zhang, J.; Yilmaz, A. S.; Jaglowski, S. M.; Blum, K. A.; Lozanski, A.; Lozanski, G.; James, D. F.; Barrientos, J. C.; Lichter, P.; Stilgenbauer, S.; Buggy, J. J.; Chang, B. Y.; Johnson, A. J.; Byrd, J. C., Resistance mechanisms for the Bruton's tyrosine kinase inhibitor ibrutinib. *N Engl J Med* **2014**, *370* (24), 2286-94.
  12. Crawford, J. J.; Johnson, A. R.; Misner, D. L.; Belmont, L. D.; Castanedo, G.; Choy, R.; Coraggio, M.; Dong, L.; Eigenbrot, C.; Erickson, R.; Ghilardi, N.; Hau, J.; Katewa, A.; Kohli, P. B.; Lee, W.; Lubach, J. W.; McKenzie, B. S.; Ortwine, D. F.; Schutt, L.; Tay, S.; Wei, B.; Reif, K.; Liu, L.; Wong, H.; Young, W. B., Discovery of GDC-0853: A Potent, Selective, and Noncovalent Bruton's Tyrosine Kinase Inhibitor in Early Clinical Development. *J Med Chem* **2018**, *61* (6), 2227-2245.
  13. Binnerts, M. E.; Otipoby, K. L.; Hopkins, B. T.; Bohnert, T.; Hansen, S.; Jamieson, G.; Howland, P. A.; Bjerkholt, E. H.; Thomas, D. A.; Fox, J. A.; Craig, A. R., Abstract C186: SNS-062 is a potent noncovalent BTK inhibitor with comparable activity against wild type BTK and BTK with an acquired resistance mutation. *Molecular Cancer Therapeutics* **2015**, *14* (12 Supplement 2), C186-C186.
  14. Ma, B.; Bohnert, T.; Otipoby, K. L.; Tien, E.; Arefayene, M.; Bai, J.; Bajrami, B.; Bame, E.; Chan, T. R.; Humora, M.; MacPhee, J. M.; Marcotte, D.; Mehta, D.; Metrick, C. M.; Moniz, G.; Polack, E.; Poreci, U.; Prefontaine, A.; Sheikh, S.; Schroeder, P.; Smirnakis, K.; Zhang, L.; Zheng, F.; Hopkins, B. T., Discovery of BIIB068: A Selective, Potent, Reversible Bruton's Tyrosine Kinase Inhibitor as an Orally Efficacious Agent for Autoimmune Diseases. *J Med Chem* **2020**.
  15. Watterson, S. H.; De Lucca, G. V.; Shi, Q.; Langevine, C. M.; Liu, Q.; Batt, D. G.; Beaudoin Bertrand, M.; Gong, H.; Dai, J.; Yip, S.; Li, P.; Sun, D.; Wu, D. R.; Wang, C.; Zhang, Y.; Traeger, S. C.; Pattoli, M. A.; Skala, S.; Cheng, L.; Obermeier, M. T.; Vickery, R.; Discenza, L. N.; D'Arienzo, C. J.; Zhang, Y.; Heimrich, E.; Gillooly, K. M.; Taylor, T. L.; Pulicchio, C.; McIntyre, K. W.; Galella, M. A.; Tebben, A. J.; Muckelbauer, J. K.; Chang, C.; Rampulla, R.; Mathur, A.; Salter-Cid, L.; Barrish, J. C.; Carter, P. H.; Fura, A.; Burke, J. R.; Tino, J. A., Discovery of 6-Fluoro-5-(R)-(3-(S)-(8-fluoro-1-methyl-2,4-dioxo-1,2-dihydroquinazolin-3(4H)-yl)-2-methylphenyl)-2-(S)-(2-hydroxypropan-2-yl)-2,3,4,9-tetrahydro-1H-carbazole-8-carboxamide (BMS-986142): A Reversible Inhibitor of Bruton's Tyrosine Kinase (BTK) Conformationally Constrained by Two Locked Atropisomers. *J Med Chem* **2016**, *59* (19), 9173-9200.
  16. Reiff, S. D.; Mantel, R.; Smith, L. L.; Greene, J. T.; Muhowski, E. M.; Fabian, C. A.; Goettl, V. M.; Tran, M.; Harrington, B. K.; Rogers, K. A.; Awan, F. T.; Maddocks, K.; Andritsos, L.; Lehman, A. M.; Sampath, D.; Lapalombella, R.; Eathiraj, S.; Abbadessa, G.; Schwartz, B.; Johnson, A. J.; Byrd, J. C.; Woyach, J. A., The BTK Inhibitor ARQ 531 Targets Ibrutinib-Resistant  
1300-1315.
  17. Kawahata, W.; Asami, T.; Kiyoi, T.; Irie, T.; Taniguchi, H.; Asamitsu, Y.; Inoue, T.; Miyake, T.; Sawa, M., Design and Synthesis of Novel Amino-triazine Analogues as Selective Bruton's Tyrosine Kinase Inhibitors for Treatment of Rheumatoid Arthritis. *J Med Chem* **2018**, *61* (19), 8917-8933.
  18. Kawahata, W.; Asami, T.; Irie, T.; Sawa, M., Design and synthesis of novel pyrimidine analogs as highly selective, non-covalent BTK inhibitors. *Bioorg Med Chem Lett* **2018**, *28* (2), 145-151.
  19. Brandhuber, B.; Gomez, E.; Smith, S.; Eary, T.; Spencer, S.; Rothenberg, S. M.; Andrews, S., LOXO-305, A Next Generation Reversible BTK Inhibitor, for Overcoming Acquired Resistance to Irreversible BTK Inhibitors. *Cl Lymph Myelom Leuk* **2018**, *18*, S216-S216.
  20. Crofford, L. J.; Nyhoff, L. E.; Sheehan, J. H.; Kendall, P. L., The role of Bruton's tyrosine kinase in autoimmunity and implications for therapy. *Expert review of clinical immunology* **2016**, *12* (7), 763-73.
  21. Hopkins, B. T.; Bame, E.; Bell, N.; Bohnert, T.; Bowden-Verhoeck, J. K.; Bui, M.; Cancilla, M. T.; Conlon, P.; Cullen, P.; Erlanson, D. A.; Fan, J.; Fuchs-Knotts, T.; Hansen, S.; Heumann, S.; Jenkins, T. J.; Marcotte, D.; McDowell, B.; Mertsching, E.; Negrou, E.; Otipoby, K. L.; Poreci, U.; Romanowski, M. J.; Scott, D.; Silvian, L.; Yang, W.; Zhong, M., Optimization of novel reversible Bruton's tyrosine kinase inhibitors identified using Tethering-fragment-based screens. *Bioorg Med Chem* **2019**, *27* (13), 2905-2913.
  22. Page, K. M., Validation of Early Human Dose Prediction: A Key Metric for Compound Progression in Drug Discovery. *Mol Pharm* **2016**, *13* (2), 609-20.
  23. Lovering, F.; Bikker, J.; Humblet, C., Escape from flatland: increasing saturation as an approach to improving clinical success. *J Med Chem* **2009**, *52* (21), 6752-6.
  24. Wolfe, J. P.; Buchwald, S. L., Scope and limitations of the Pd/BINAP-catalyzed amination of aryl bromides. *J Org Chem* **2000**, *65* (4), 1144-57.
  25. Shah, P.; Westwell, A. D., The role of fluorine in medicinal chemistry. *J Enzyme Inhib Med Chem* **2007**, *22* (5), 527-40.
  26. Johnson, T. W.; Gallego, R. A.; Edwards, M. P., Lipophilic Efficiency as an Important Metric in Drug Design. *J Med Chem* **2018**, *61* (15), 6401-6420.
  27. Freeman-Cook, K. D.; Hoffman, R. L.; Johnson, T. W., Lipophilic efficiency: the most important efficiency metric in medicinal chemistry. *Future Med Chem* **2013**, *5* (2), 113-5.
  28. Hopkins, A. L.; Keseru, G. M.; Leeson, P. D.; Rees, D. C.; Reynolds, C. H., The role of ligand efficiency metrics in drug discovery. *Nat Rev Drug Discov* **2014**, *13* (2), 105-21.
  29. Hansen, K.; Mika, S.; Schroeter, T.; Sutter, A.; ter Laak, A.; Steger-Hartmann, T.; Heinrich, N.; Muller, K. R., Benchmark data set for in silico prediction of Ames mutagenicity. *J Chem Inf Model* **2009**, *49* (9), 2077-81.
  30. Kazius, J.; McGuire, R.; Bursi, R., Derivation and validation of toxicophores for mutagenicity prediction. *J Med Chem* **2005**, *48* (1), 312-20.
  31. McCarren, P.; Springer, C.; Whitehead, L., An investigation into pharmaceutically relevant mutagenicity data and the influence on Ames predictive potential. *J Cheminform* **2011**, *3*, 51.
  32. Leroux, F. R.; Manteau, B.; Vors, J. P.; Pazenok, S., Trifluoromethyl ethers--synthesis and properties of an unusual substituent. *Beilstein J Org Chem* **2008**, *4*, 13.
  33. Rashid, K. A.; Arjmand, M.; Sandermann, H.; Mumma, R. O., Mutagenicity of chloroaniline/lignin metabolites in the Salmonella/microsome assay. *J Environ Sci Health B* **1987**, *22* (6), 721-9.
  34. Nohmi, T.; Yoshikawa, K.; Nakadate, M.; Miyata, R.; Ishidate, M., Jr., Mutations in Salmonella typhimurium and inactivation of Bacillus subtilis transforming DNA induced by phenylhydroxylamine derivatives. *Mutat Res* **1984**, *136* (3), 159-68.
  35. Dowty, M. E.; Lin, J.; Ryder, T. F.; Wang, W.; Walker, G. S.; Vaz, A.; Chan, G. L.; Krishnaswami, S.; Prakash, C., The pharmacokinetics, metabolism, and clearance mechanisms of tofacitinib, a janus kinase inhibitor, in humans. *Drug Metab Dispos* **2014**, *42* (4), 759-73.

**Declaration of interests**

The authors declare that they have no known competing financial interests or personal relationships that could have appeared to influence the work reported in this paper.

The authors declare the following financial interests/personal relationships which may be considered as potential competing interests:

Journal Pre-proofs